SEMICONDUCTION IN METAL-DOPED PYROPOLYMERS

By

STEVEN DAVID HOTTMAN

Bachelor of Science

Oklahoma State University

Stillwater, Oklahoma

1969

Submitted to the Faculty of the Graduate College
of the Oklahoma State University
in partial fulfillment of the requirements
for the Degree of
MASTER OF SCIENCE
July, 1970

SEMICONDUCTION IN METAL-DOPED

PYROPOLYMERS

Thesis Approved:

Herbert A. Pohl
Thesis Adviser

Joel J. Martin

D. Durham
Dean of the Graduate College

ACKNOWLEDGEMENTS

The author would like to express his heart-felt thanks to Dr. H. A. Pohl for his time and effort spent in discussion and guidance throughout this study. The author would also like to thank Dr. J. R. Wyhof for his helpful discussions and encouragement. Thanks also go to Dr. W. J. Leivo and Mr. W. Steckelberg for their help in the x-ray studies. The author is indebted to Dr. J. N. Lange and his students for helpful discussion and use of equipment. Special thanks go to Mr. H. Hall and his associates in the Chemistry-Physics machine shop for the construction of equipment.

Financial support for this study was furnished by the U. S. Army Mobility Equipment Research and Development Center, and the Paint Research Institute, which the author gratefully acknowledges. Special thanks go to the National Science Foundation for the grant of a Research Traineeship.

The author would also like to thank Mrs. Linda Schroeder for typing the manuscript. Finally, special thanks go to my wife, Susan, for her understanding and encouragement.

TABLE OF CONTENTS

LIST OF TABLES

LIST OF FIGURES

CHAPTER I

INTRODUCTION

In the past decade much attention has been given to organic semiconductors. More recently a group of materials within the class of organic semiconductors has begun to receive more attention. These are pyropolymers. They are formed by heating various organic starting materials to temperatures between 500°C and 1200°C. The resulting polymers exhibit resistivities between 10^{10} ohm-cm and 10^{-3} ohm-cm. The purpose of this study is to investigate the conduction process of several of the metal-doped pyropolymers.

There was considerable work done on graphites and doped graphites before the middle of the century (1-8). In general it was thought that the dopants distorted the graphite lattice and the graphite band structure.

Somewhat later Pohl and coworkers at Princeton became interested in the similar metal-doped polymer carbons. These materials were formed by pyrolyzing metal loaded ion-exchange resins to temperatures of 700°C to 1200°C (9-12). They found the resistivity to generally decrease as the heat treatment temperature or the impurity concentration was increased. However, in some cases a slight increase in resistivity was noted as the doping level was raised. This was attributed to increased scattering, but was by and large not given any emphasis in the final analysis. Dopants included nickel (9); sodium, calcium, and

thorium (11); and aluminum (12). Resistivities of the order of 10^{-1} ohm-cm to 10^{-2} ohm-cm and Hall mobilities of 1-4 $cm^2/v\text{-}sec$ were observed. Activation energies of-0.005 eV to 0.05 eV were found.

The above materials were all analyzed using the conventional band concepts associated with crystalline samples. However, it has been pointed out (16-19) that much of the data can be interpreted using a non-crystalline model; that is, a model without long range order. The accompanying concepts of valence and conduction bands, Fermi surface, and wave-functions with well defined wave lengths has been used to understand apparently anomolous data (20, 21).

Mott has been quite active in the area of non-crystalline conduction. He has studied in some detail many amorphous systems, including certain thin films, glasses, and polycrystalline materials (16-18, 21, 22). He suggests a hopping or tunneling mechanism for conduction very similar to impurity conduction in doped and compensated crystalline semiconductors (22). He also suggests criteria for the localization of energy states leading to the thermally activated tunneling mechanism (22, 23). He has given the connection between polaron formation and hopping conduction (24).

Lifshitz has done considerable work in the field of disordered systems, particularly on the energy spectra in various models (25).

Several experimental anomalies have been resolved by Böer. He suggests the reason for the large difference between the measured Hall mobility and the drift mobility calculated from conductivity and carrier concentration data in highly disordered semiconductors (26-28). He states that if 1) the mean free path of the carrier is of the order of, or less than the lattice constant, or if 2) the material is highly

inhomogeneous as in a polycrystalline sample, or if 3) the material is highly compensated, the Hall mobility may be orders of magnitude lower than the drift mobility. In the first two cases he attributes this to large potential perturbations which are superimposed on the external field and which contribute the major field seen by the carrier. In the third case, he tentatively attributes the difference to a difference in the effective masses of the holes and electrons at a given energy.

Of considerable interest is the method used to measure the resistivity. The early experiments were performed on single crystal samples so that the standard four-point probe method was easily used. Later, powdered or polycrystalline materials became of interest, and new methods were developed. McDonnell, et al, (6) compacted and measured their samples under a small constant load. Pohl and others (10-12) formed their samples into small briquets, using a low ash phenolic binder. Recently methods have been perfected which use the response of an AC circuit to deduce the bulk resistivity of both single crystal and polycrystalline materials (13). Also, methods utilizing high pressure (10-40 kbar) have been used (14, 15).

In this study, the resistivity, activation energy, and thermoelectric power were measured for several potassium- and lithium-doped pyropolymers. These data, and structural information gained from the x-ray studies, will be used to examine the conduction mechanisms of the materials.

CHAPTER II

EXPERIMENTAL MATERIALS AND TECHNIQUES

Sample Preparation

The metal-doped polymers were prepared using the technique of Ottmers and Rase (29), in which stoichiometric amounts of the polymer carbon and the dopant are mechanically mixed in an inert atmosphere to a temperature of 275°C $\pm$ 25°. The entire process of preparing, weighing, and reacting the materials was carried out in an inert atmosphere. All measurements were made in an ambient atmosphere. Tests on highly doped samples showed no change in properties over a five-hour period in an ambient atmosphere.

The pyropolymer carbon was prepared in the following manner. A prepolymer was formed by heating crystalline sucrose ($C_{12}H_{22}O_{11}$) to a temperature of 200°C to 300°C in a nitrogen atmosphere. The heating was continued for at least 24 hours. After this period of heating a coarse, black material, approximately 90% carbon (30) remained. This material was then heated to the appropriate heat treatment temperature, T_H, of 600°C to 1200°C under a steady flow of helium gas.

During the heat treatment the highly volatile compounds are first driven off, and the residual material forms a larger partially dehydrogenated molecules. At about 700°C small crystallites begin to form; these grow from ~10 Å in diameter at 700°C to ~3000 Å in diameter at

3000°C. Between 600°C and 800°C the resistivity decreases very rapidly; above this temperature the resistivity decreases only slowly with increased temperature. This is due to a balance between the decrease in unpaired electrons with reside at the crystallite edges and the increase in crystallite size which decreases boundry scattering (31).

Resistivity Measurements

All 600°C polymers were measured using a Bridgeman opposed anvil method (32) (see Figure 1). A pyrophylite retaining ring was placed on the face of the lower anvil and a small amount of polymer was placed in the ring. The upper anvil was placed in position and a pressure of approximately 10 kbar was applied. This removed any voids in the sample (33). Resistance measurements were made as a function of pressure using a Simpson model 269 multimeter. At the end of a run the sample thickness was determined; this and the resistance measurements gave the polymer resistivity from the equation

$$\rho = \frac{RA}{t} \tag{1}$$

where R is the resistance, A the cross-sectional area in cm^2, and t the thickness in cm.

The 800°C, 1000°C, and 1200°C polymers were measured using a technique suggested by van der Pauw (34). The method utilizes a new modification of the Chester-Jones (35) type clamp. It was constructed of Delrin with four platinum resistance probes embedded in the lower anvil face (see Figure 2). Van der Pauw derived the expression for the resistivity of a circular sample with four point probes, A, B, C, and D, around the periphery:

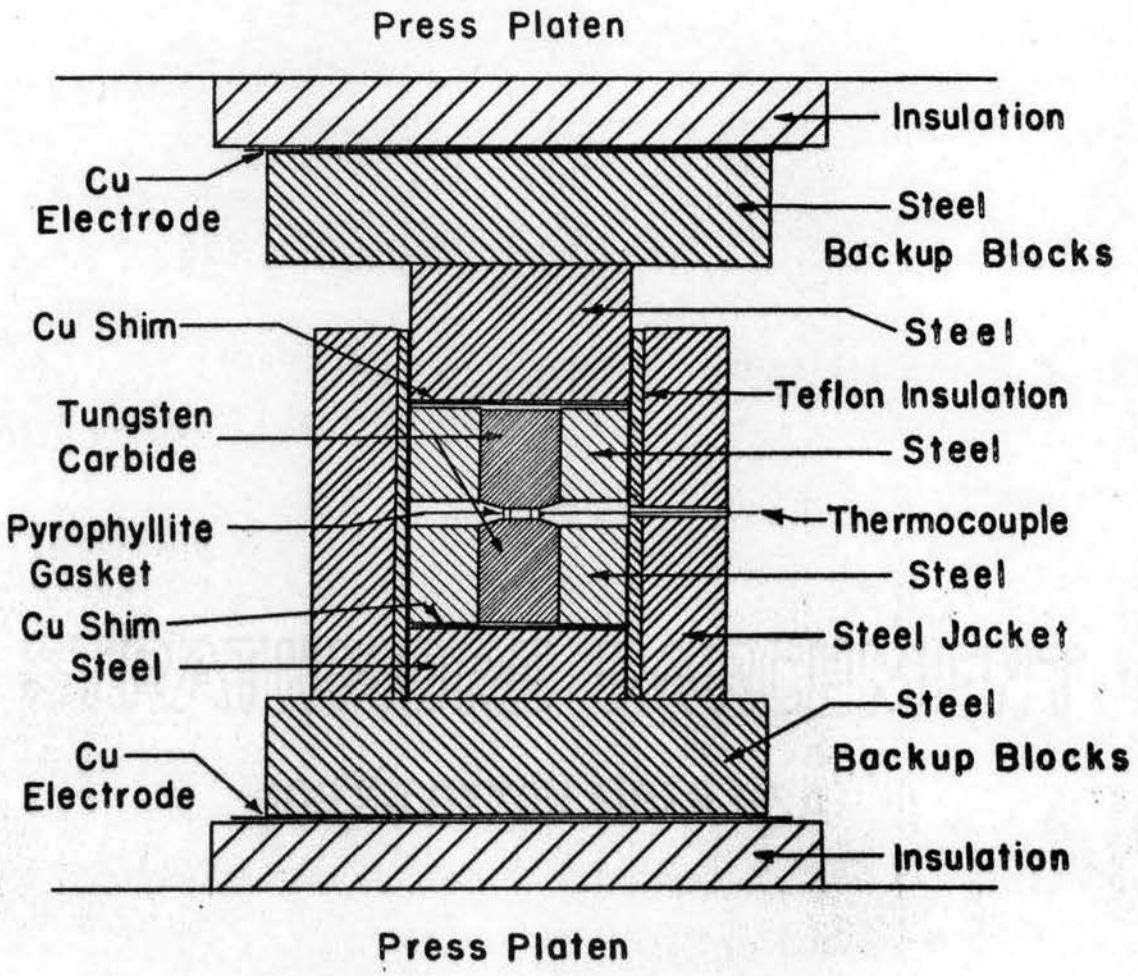

Figure 1. High Pressure Resistivity Cell

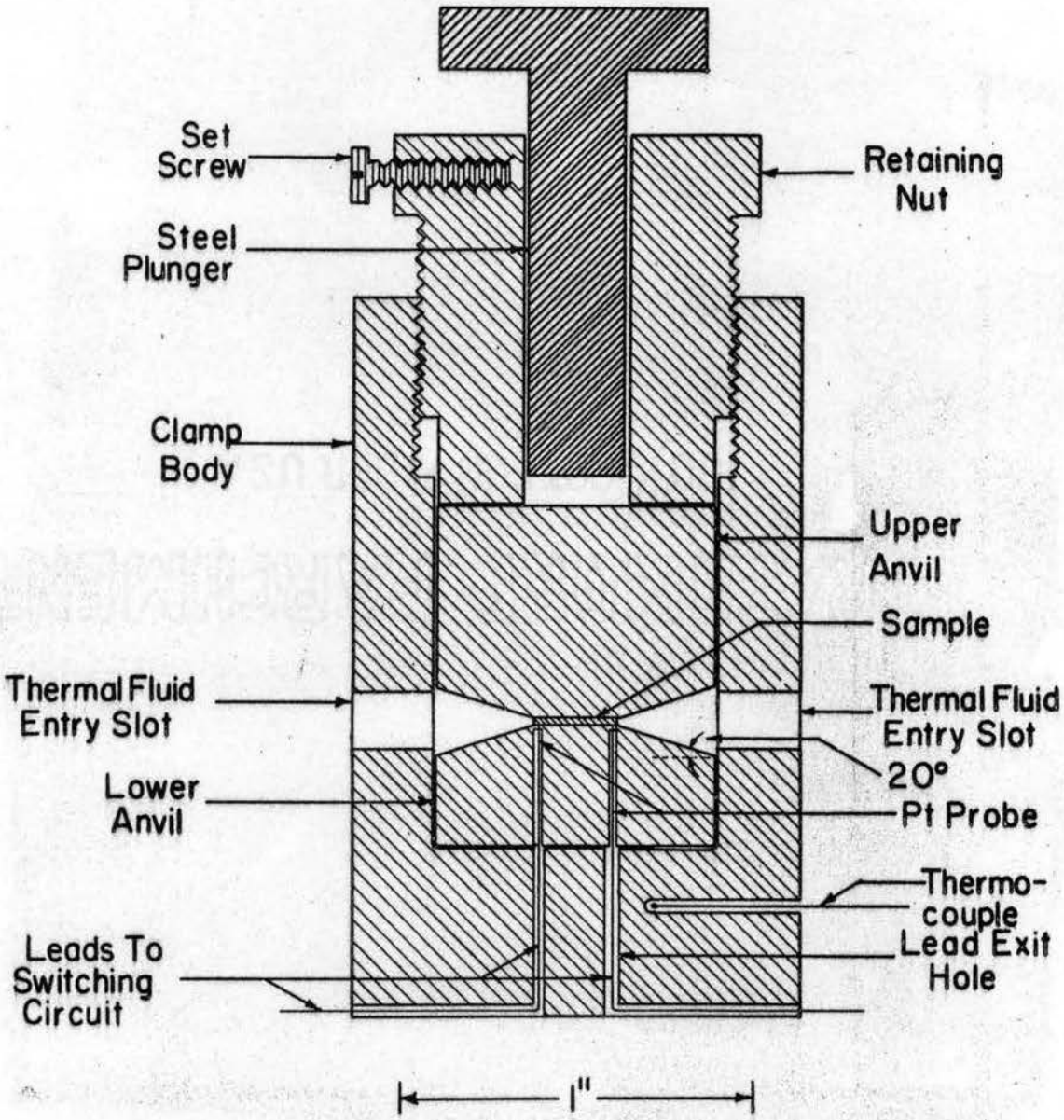

Figure 2. Four-Point Probe Pressure Clamp

$$\rho = \frac{\pi t}{\ln 2} \left[\frac{R_{AB,CD} + R_{BC,DA}}{2}\right] \cdot f \qquad (2)$$

where $R_{AB,CD}$ is the potential drop $V_D - V_C$ between contacts D and C per unit current through contacts A and B, and f is a function of the ratio $R_{AB,CD}/R_{BC,DA}$ only; for the ratio between 1 and 2, f is very nearly unity, and in most cases was not used. The error introduced by the probes being placed a distance d from the edge of the sample is proportional to d^2/D^2, where D is the sample diameter. For the dimensions of the cell used this error was less than 1%.

In practice voltage-current ratios were taken at all of the four cyclic permutations of (AB,CD), and a pair-wise average was taken as the polymer resistivity. The circuit shown in Figure 3 is used to change contacts.

Samples measured in the four-point probe clamp were initially premolded between tungsten carbide anvils to a pressure of approximately 8.5 kbar to remove voids. This premolded pellet was then placed between the Delrin anvils of the clamp, and the clamp assembly was placed in the hydraulic press, a 12-½ ton Model SB 240 Pasadena Hydraulic Inc. press. The press load was increased in increments of 250 to 500 pounds and resistivity data was taken at each load. These and resistivity measurements made after tightening the retaining nut gave the ambient pressure in the clamp.

The potential drop was measured with a Leeds and Northrup K-4 potentiometer, with a sensitivity of at least 10^{-6} volts. Current measurements were made with a Keithley 610B electrometer, with an accuracy of better than 1%. Figure 4 shows the experimental circuit.

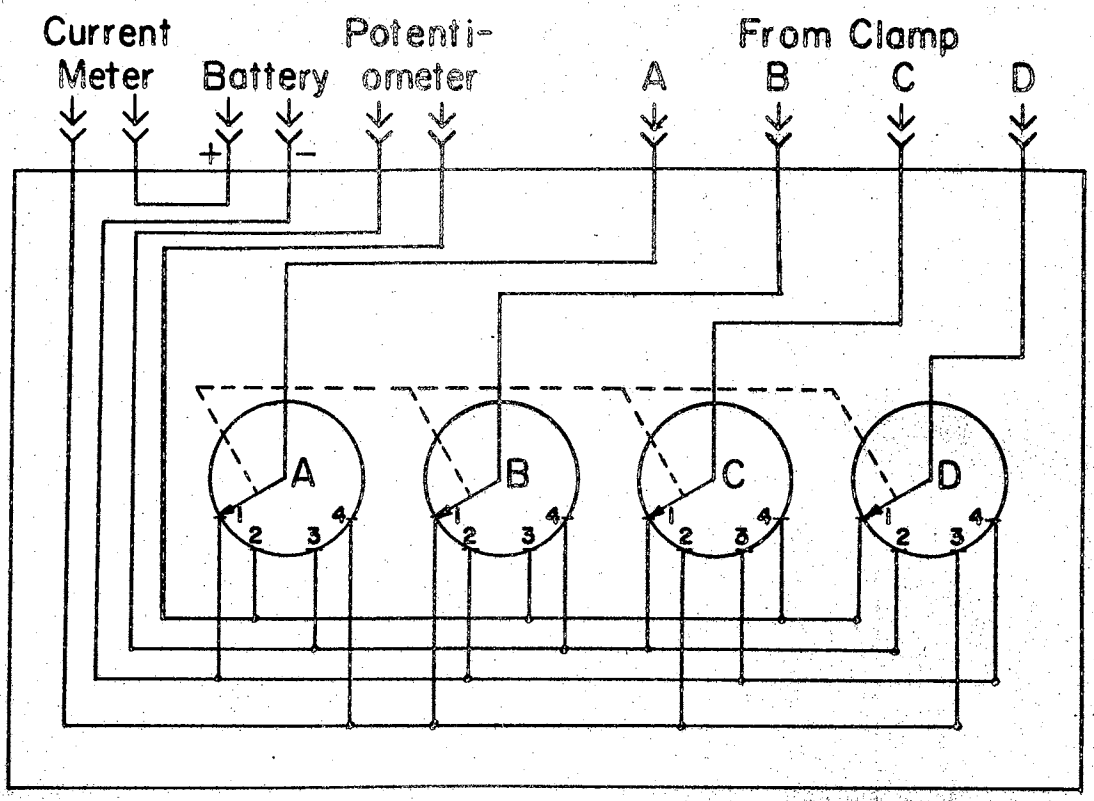

Figure 3. Four-Point Probe Switching Circuit

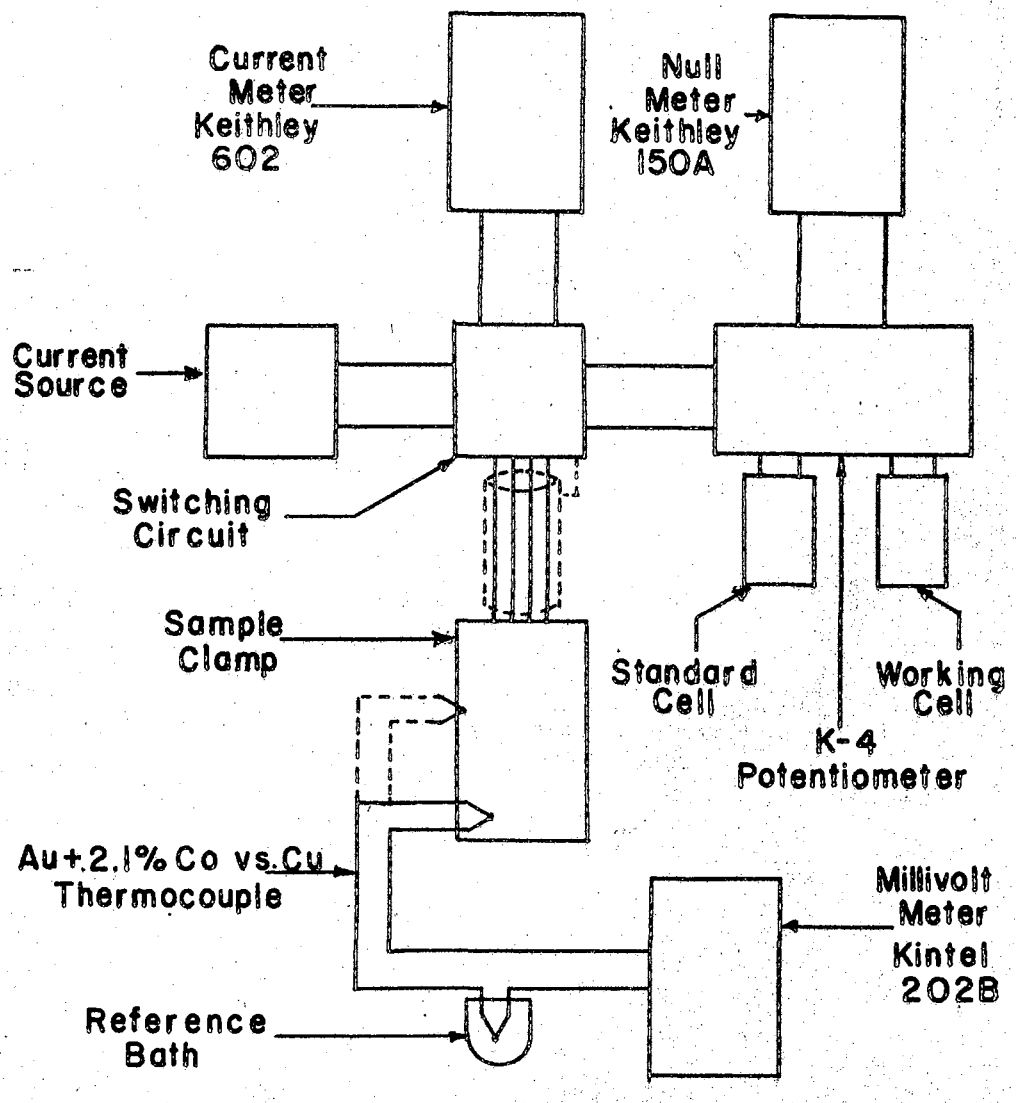

Figure 4. Block Diagram of the Resistivity Measurement System

Activation Energy

The conduction activation energy was determined for each sample. A semiconductor often obeys the equation

$$\rho = \rho_o e^{E_a/kT} \tag{3}$$

(36) where ρ_o is a constant of the material, E_a the activation energy, k is the Boltzmann's constant, and T the absolute temperature. A plot of log versus T^{-1} should give a straight line which has a slope of E_a/k.

Most samples were measured in the temperature range of 300°K to 77°K; a few were measured in the range of 300°K to 1.7°K. For these latter samples, the four-point probe clamp was placed in the liquid helium cryostat (Figure 5). The cryostat was constructed so that the vapor pressure above the cryogenic liquid could be lowered and thereby obtain lower temperatures.

When using the Delrin four-point probe clamp it was necessary to allow about 1/2 hour for the entire clamp to come to thermal equilibrium; otherwise differential thermal expansion of the Delrin would produce unknown pressures in the clamp. By using two thermocouples, one buried in the interior of the clamp and the other on the surface, the time to reach equilibrium was found to be ~30 minutes in liquid nitrogen. This was the minimum time between measurements at different temperatures.

The temperature of the sample was usually determined from vapor pressure-temperature data of the liquid nitrogen or helium. A (gold-2.3At% cobalt) versus copper thermocouple was calibrated and used occasionally. A computer program was used to fit a cubic equation through three known temperature-emf points for the calibration.

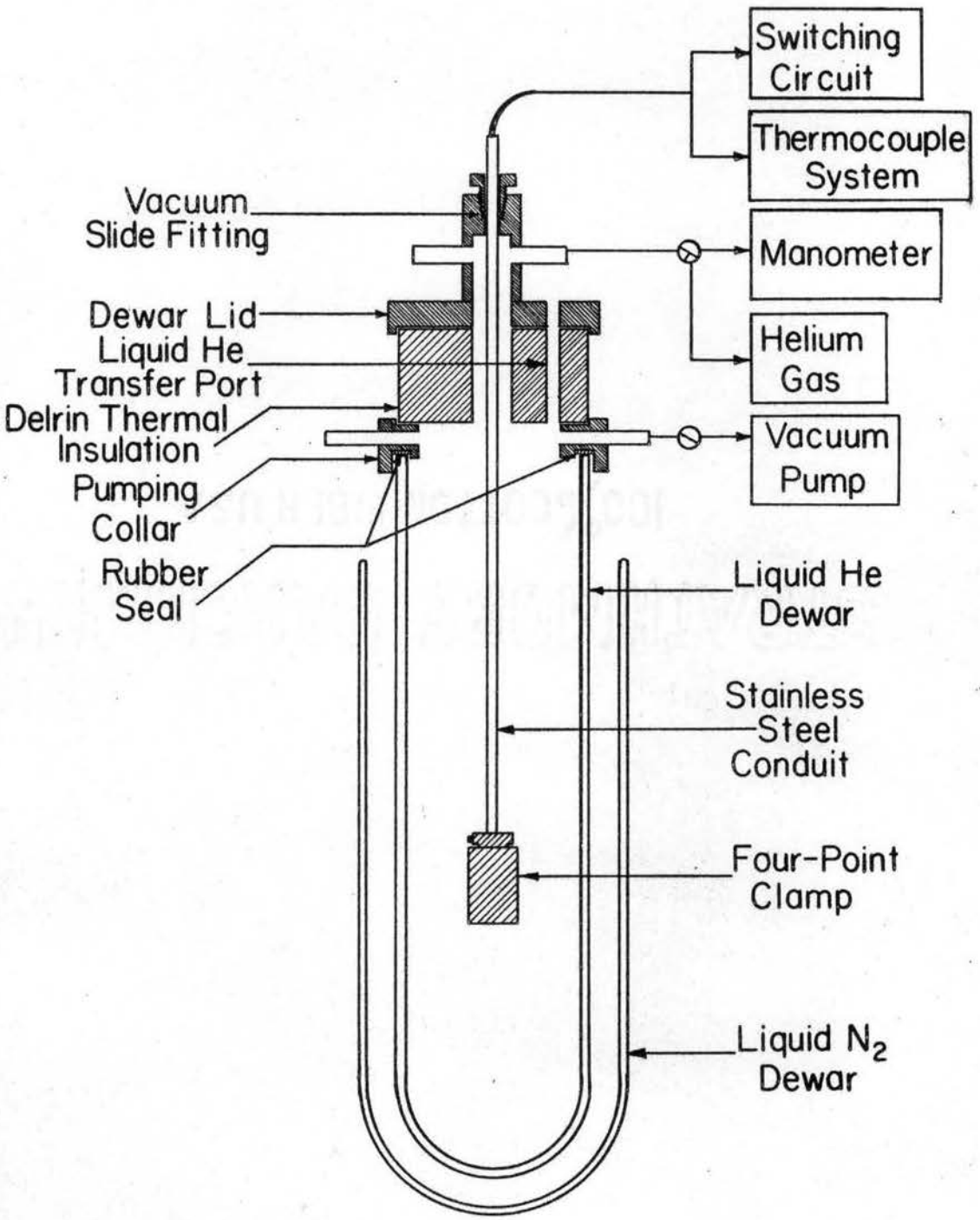

Figure 5. Liquid Helium Dewar

Electron Spin Resonance

Electron spin resonance studies were carried out on all of the 1000°C polymers in order to determine any correlation between spin concentration and conductivity. The instrument was an Alpha Scientific Laboratory Model AL 340 SY Electron Spin Resonance Spectrometer. It used a 60 Hz sweep and 100 kHz modulation of the magnetic field; the sensitivity was of the order of 10^{15} spins/gauss line width.

Microgram quantities of α , α-diphenyl-β-picryl hydrazyl (DPPH) were used as the primary standards (37); secondary standards were made from stable dilutions of polymer and tin oxide (41).

The polymers to be measured were placed in Vycor sample tubes equipped with vacuum stop-cocks. The samples were then out-gassed at a pressure of less than 10^{-5} mm Hg for at least 24 hours. While being evacuated the samples were heated to ~65°C to aid in the removal of adsorbed gases. The samples were weighed before and after the out-gassing.

The spin concentration was determined by comparing the output curve of the sample with that of the standard. The output was a recorder trace which corresponded with the first derivative of the adsorption curve of the sample (38) (see Figure 6). For each curve the product of the curve height, h , and the square of the halfwidth of the curve, $(\Delta H_{\frac{1}{2}})^2$, were computed. These products, the sample weight, w , and the spins in the standard, s , give the spin concentration, S , from

$$S = \frac{[h\Delta H_{\frac{1}{2}}^2]_{\text{unknown}}}{[h\Delta H_{\frac{1}{2}}^2]_{\text{standard}}} \times \frac{s}{w} \qquad (4)$$

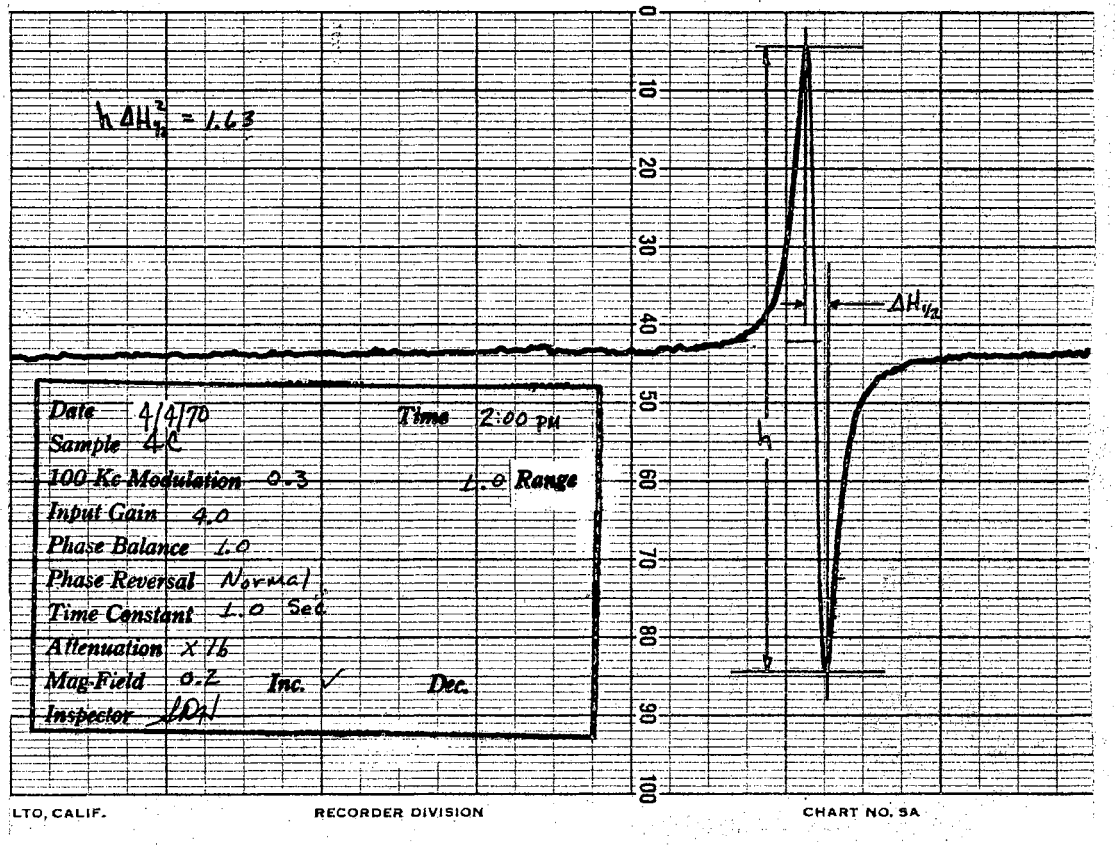

Figure 6. Electron Spin Resonance Line for DPPH Standard

The halfwidth of the curve was converted from a distance on the output chart to gauss by means of the recorder constant, R = 7.072 gauss/cm.

The low temperature spin concentrations were determined in a similar manner. The samples, standards, and resonance cell were maintained at 77.4°K by a liquid nitrogen bath. Since the DPPH standard is a stable free radical, there was no change in spin concentration due to the lowering of the temperature.

Thermoelectric Power

Measurements of the absolute thermoelectric power were made on the 1000°C samples. Figure 7 shows the apparatus used. The thermoelectric voltage generated by the temperature difference was measured with a Leeds and Northrup K-4 potentiometer through the platinum arm of the platinum versus platinum-10% rhodium thermocouples welded to the platinum foil. These voltages were the thermoelectric voltages of the sample versus platinum. The absolute values were determined by correcting the voltages measured by the thermoelectric voltage of the platinum at the given temperature. The thermoelectric power, Q , is the ratio of the thermoelectric voltage, $\mathcal{E}_t$, to the temperature difference, ΔT , between the platinum leads (33):

$$Q = \frac{\mathcal{E}_t}{\Delta T} \qquad (5)$$

The thermoelectric power was determined at a number of sample temperatures between 25°C and 115°C. Sample temperatures were determined with a copper versus constantan thermocouple near the sample. Temperature differences ranged from ~10°C to ~60°C across the sample.

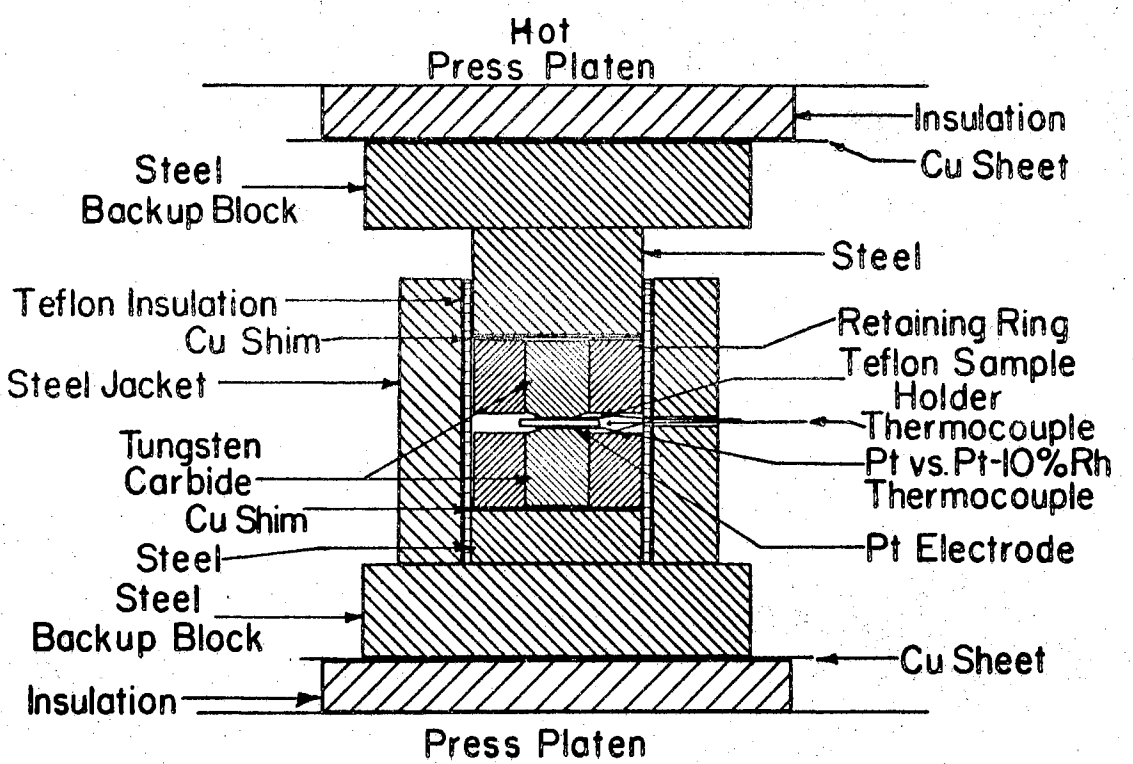

Figure 7. Thermoelectric Power Measurement Cell

X-ray

X-ray diffraction measurements were made on several of the polymers. Powder diffraction techniques were used with a forward reflection camera. A General Electric Model CA-7 x-ray machine with a copper target was used at a voltage of 45 kv and a plate current of 15 ma. Exposures ranged from 15 minutes for thin samples to 75 minutes for thicker samples; the film was Kodak type NS-54T x-ray film. The sample was mounted on a lead shield over a hole ~2 mm on a side. The sample was placed near the end of the beam collminator, a distance of 4.1 cm from the film.

The relation

$$\Theta = \frac{1}{2} \tan^{-1}\left(\frac{r}{D'}\right) \tag{6}$$

gives the Bragg angle Θ, where r is the diffraction ring radius and D' is the distance from the sample to the film. The distance between diffracting layers, d, is then calculated from

$$d = \frac{1}{2} \lambda \frac{1}{\sin \Theta} \tag{7}$$

where λ is the wavelength of the x-rays; here $\lambda = 1.54$ Å.

The Scherrer relation,

$$D = \frac{K \lambda}{\beta \cos \Theta}, \tag{8}$$

is used to estimate the crystallite size, D. β is the diffusion angle of the ring and $K \sim 1$ is a parameter depending on the crystallite shape (39).

CHAPTER III

RESULTS AND DISCUSSION

Since all of the polymers were measured under pressure it is useful to have some information concerning the polymers' behavior as a function of pressure. Figure 8 shows the resistivity as a function of the square root of the pressure. Units of $P^{\frac{1}{2}}$ are chosen for the ordinate since theory (14) predicts a straight-line dependence for resistivity as a function of $P^{\frac{1}{2}}$. It is seen that above a pressure of ~1.4 kbar ($P^{\frac{1}{2}} \approx 1.2$ kbar$^{\frac{1}{2}}$) the resistivity does behave in such a manner. This is taken as an indication that all voids have been eliminated and that the contact potentials are essentially constant above this pressure. That is, the bulk properties are being measured beyond some critical pressure, which is less than 2 kbar. With these considerations in mind a standard pressure of 2 kbar was chosen for all further resistivity measurements. This pressure was easily obtained with the four-point probe clamp.

Figure 9 shows the resistivity at 2 kbar and 297°K as a function of heat treatment temperature, T_H, for three representative doping levels. As expected, the resistivity drops quite rapidly for heat treatment temperatures between ~600°C and ~800°C. Between ~800°C and ~1000°C the change is slower, and by ~1200°C the change is quite slow. As mentioned in Chapter II, this behavior is due to two opposing changes: the growth of the crystallites and the destruction of the

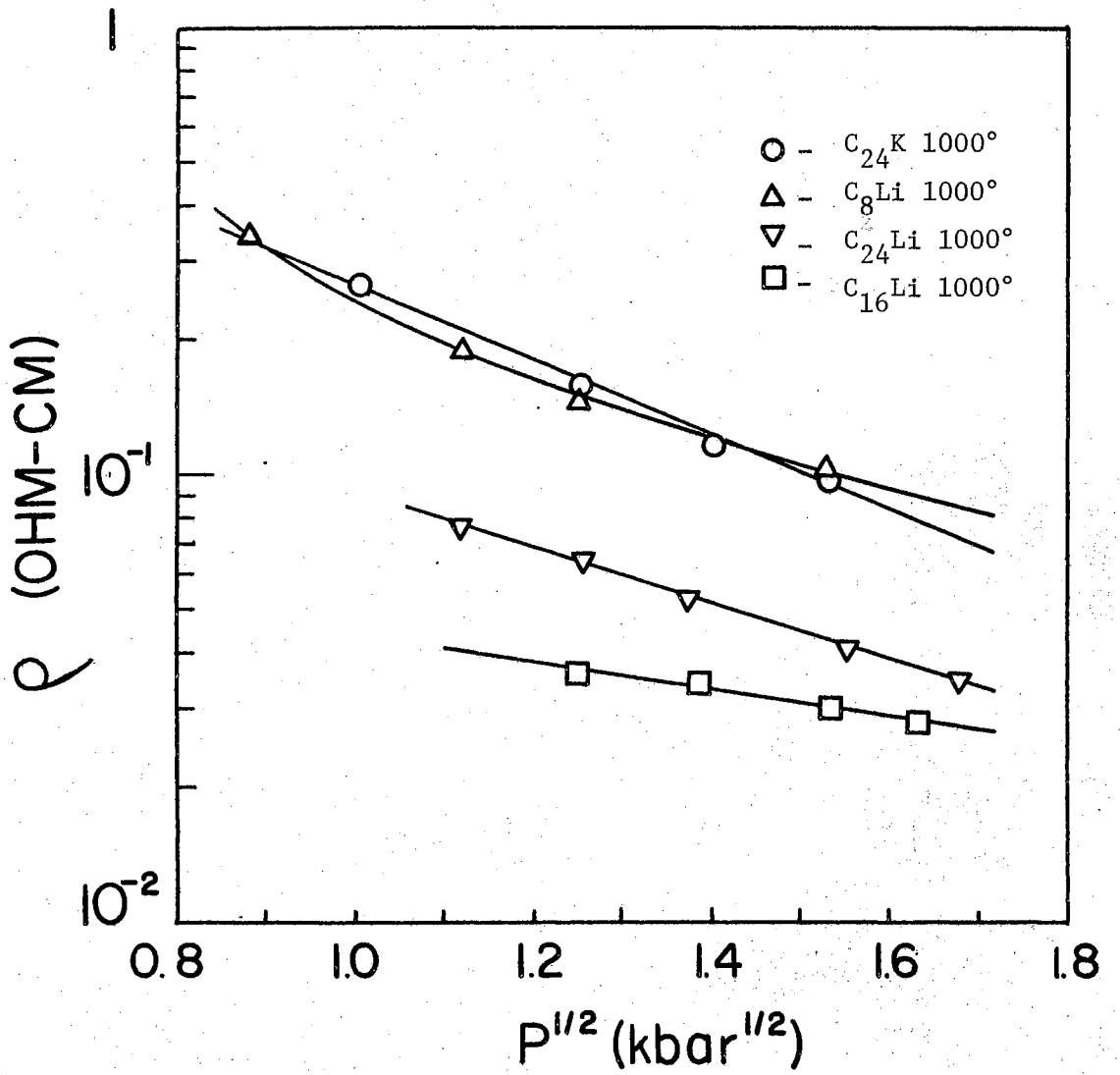

Figure 8. ρ Versus $P^{\frac{1}{2}}$ for Polymers 3C, 13C, 14C, and 15C Showing Linear Dependence Above P = 1.4 kbar. T = 297°K

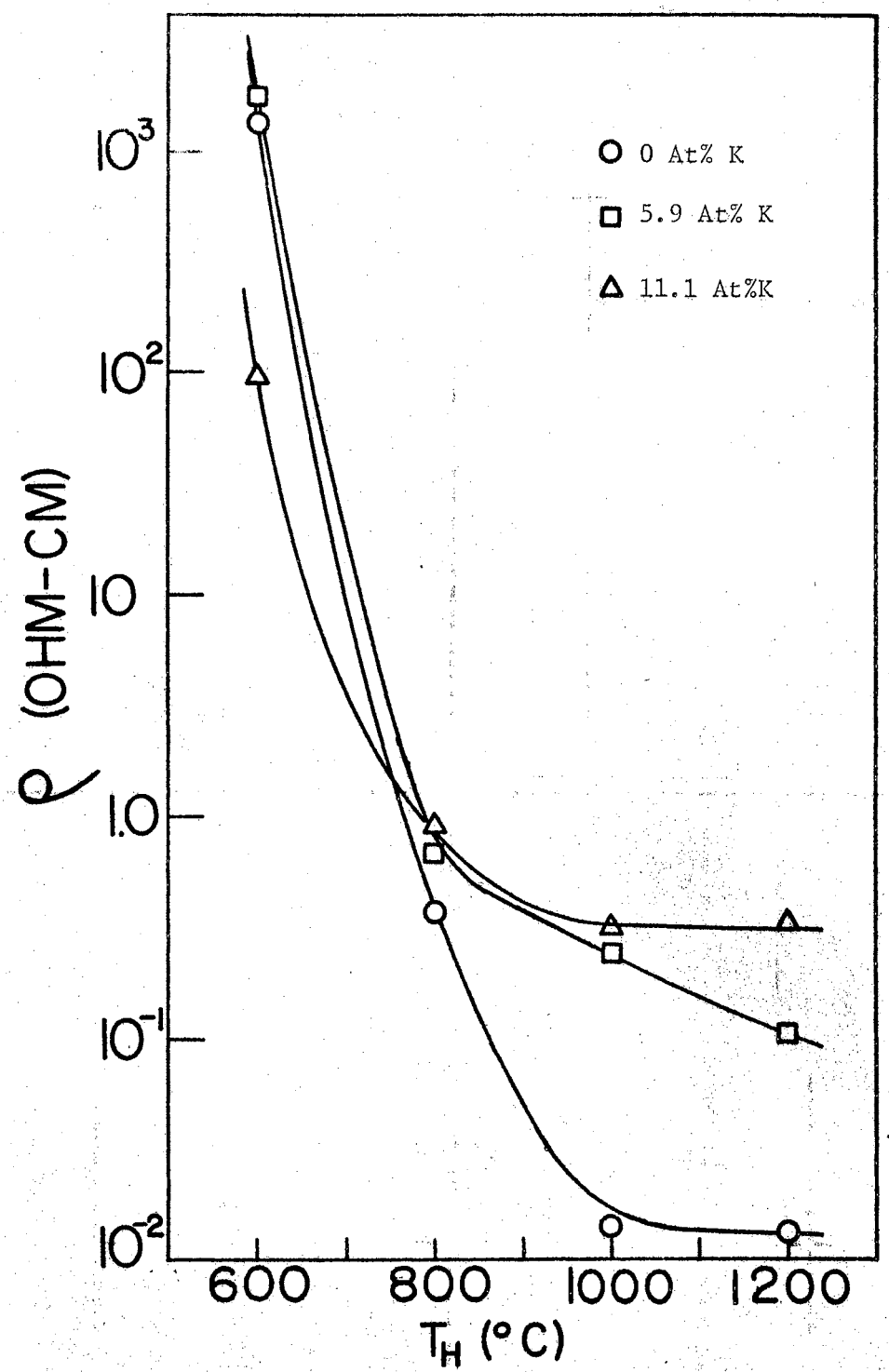

Figure 9. ρ Versus T_H for Undoped, 5.9 At%K, and 11.1 At% K Polymers. P = 2 kbar, T = 297°K

edge radicals. As T_H is increased between 600°C and 800°C, large numbers of edge radicals, and therefore carriers, are generated. This leads to a rapidly decreasing resistivity. Between 800°C and 1000°C only relatively few carriers are added to the large total number. However, in this range the growth of the crystallites begins to become important, and the resistivity is further decreased as the crystallites grow. Above a T_H of 1000°C, the destruction of edge radicals by the combination of crystallite edges as the crystallites grow is essentially balanced by the increased mobility permitted by the larger crystallite dimension. This results in a leveling off of the resistivity as a function of heat treatment temperature.

The x-ray data, Table I, supports this crystallite growth hypothesis. The diffuse ring widths give an indication of the crystallite size, D . Powdered graphite is included for reference. X-ray diffraction work of others (42, 43) also supports this general growth pattern.

The same general pattern holds for the doped polymers. In these materials, however, the metal dopant probably acts as a scattering center resulting in an increased resistivity.

The diffraction photographs tend to indicate that the polymers are either solutions or compounds, and not bulk mixtures, of carbon and the bulk metal. If there were a distribution of bulk metal in the samples there would be a superposition of the carbon and metal diffraction patterns. This was not seen. However, in some cases where the metal concentration was high there were faint rings giving a separation of approximately the ionic diameter of the appropriate metal.

TABLE I

X-Ray Diffraction Results Giving Distances Calculated from Strong and Faint Diffraction Rings. Estimate of Crystallite Size Calculated from Dispersion of Strong Rings

Sample	Strong Rings (Å)	Faint Rings (Å)	D(Å)
Graphite	3.4, 2.3, 2.1	4.6, 2.8, 1.9	~90
600°C Undoped	4.5	---	7.0
800°C Undoped	4.2	2.2	8.4
1000°C Undoped	4.2	2.2	8.0, 4.9
1200°C Undoped	5.8	2.2	9.0
1000°C C_8K	3.2, 2.9	2.5	5.3-6.5, 8.5-10.0
1000°C $C_{16}K$	2.9	7.1, 3.1, 2.2, 2.4	
1000°C $C_{24}K$	3.1, 2.8	6.9, 4.0, 3.4, 2.4, 2.2	
1000°C $C_{36}K$	2.8	6.6, 3.8, 3.0, 2.4	
1000°C C_8Li	2.8	4.1, 2.2	
1000°C $C_{16}Li$	4.3	2.8, 2.1	
1000°C $C_{24}Li$	3.9, 2.8	2.2	
1000°C $C_{51}Li$	4.2	2.8, 2.1	

The resistivity as a function of doping level supports the hypothesis that the materials are compounds or solutions. Figure 10 shows the resistivity as a function of the doping level. If the samples were mixtures, one would expect the resistivity to behave as a weighted average of the resistivities of the two materials, i.e., a decrease in resistivity with increased metal concentration would be expected.

However, it is seen that the resistivity increases with metal concentration. Figure 11 shows the resistivity as a function of the electron donor concentration, N_D . From the discussion in Chapter II and above, carriers are produced by a reaction of the type

$$2C \rightleftharpoons C^+ + C_b^- = e^+ + e^- = e^+ + I \tag{9}$$

and the metal dissociates as

$$M \rightleftharpoons M^+ + e^- \tag{10}$$

where C^+ is a mobile positive carrier, or "hole", C_b^- is a bound negative ion, I is the impurity concentration, and M and M^+ are the metal and metal in concentrations, respectively. Neutrality gives, in the undoped case,

$$n_o + I_o = p_o \ , \tag{11}$$

and in the doped case,

$$n + I = p + M^+ \tag{12}$$

where n is the electron concentration, and p is the hole concentration; the zero subscript refers to the undoped case throughout.

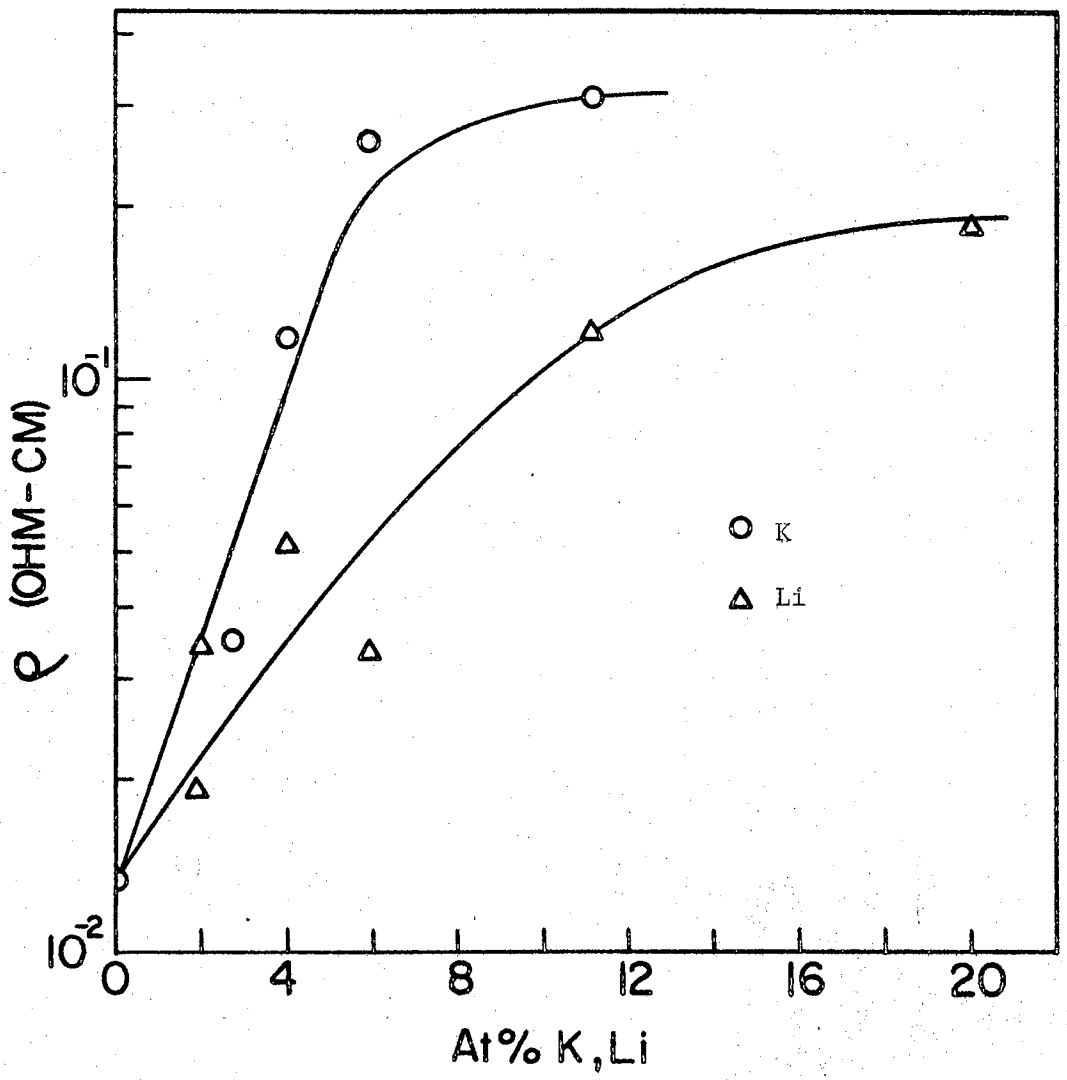

Figure 10. ρ Versus At% K, Li for 1000°C Polymers. P = 2 kbar, T = 297°K

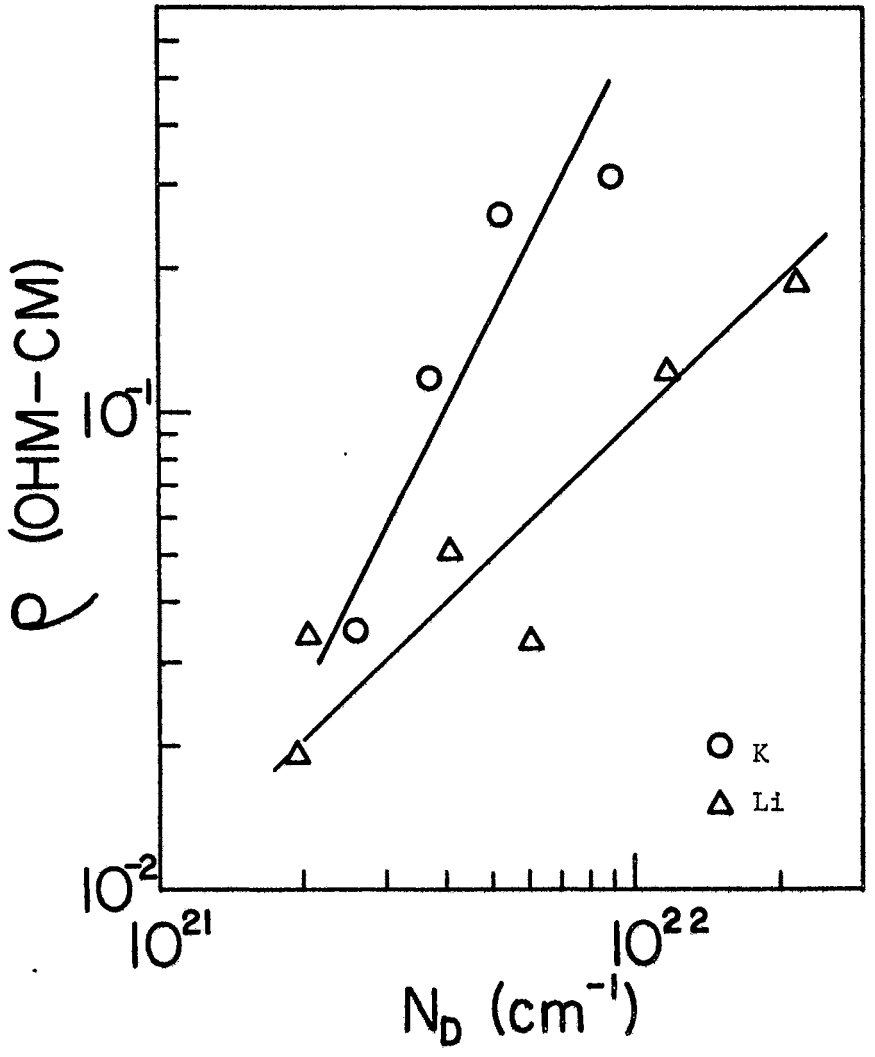

Figure 11. ρ Versus N_D for 1000°C Potassium and Lithium Polymers. P = 2 kbar, T = 297°K

From Eq. (9),

$$K_\ell = \frac{n_o p_o}{C_{\ell o}^2} = \frac{np}{C_\ell^2} \tag{13}$$

where K_ℓ is the lattice carrier concentration product, and the C_ℓ are lattice carbon concentrations.

For low ionization, $C_{\ell o}^2 \cong C_\ell^2$ (14)

and $n_o p_o = np = K_\ell C_\ell^2 \cong K_L$ (15)

Likewise, the bound dissociation constant, K_B, is given by

$$K_B = K_b C_\ell = \frac{p_o I_o}{C_{bo}} = \frac{pI}{C_b} \quad . \tag{16}$$

If α is the fraction of edge ions ionized, then $1 - \alpha$ is the fraction unionized, and

$$I = \alpha C_b \simeq C_b \simeq I_o \tag{17}$$

and $$C_{bo} = (1 - \alpha) C_b \quad . \tag{18}$$

Then $$\frac{p_o \alpha_o}{(1 - \alpha_o)} = \frac{p\alpha}{(1 - \alpha)} = K_B \tag{19}$$

and if $\alpha \simeq 1 \simeq \alpha_o$,

$$\frac{p_o}{1 - \alpha_o} \cong \frac{p}{1 - \alpha} \tag{20}$$

Similarly for the metal atoms, where β is the fraction of metal atoms ionized,

$$\frac{n}{(1 - \beta)} = \frac{n_o}{(1 - \beta_o)} = K_M \tag{21}$$

and $$M^{+} \cong M \ , \tag{22}$$

From Eqs (11), (12), (15), and (22), we get

$$(p_o - I_o)p_o = (p + M - I)p = K_L \ ; \tag{23}$$

from Eq (18), $$(p_o - I_o)p_o \cong (p + M - I)p \tag{24}$$

or $$p^2 + (M - I)p - p_o(p_o - I) = 0 \tag{25}$$

Therefore, $$p = \frac{(I - M) + \sqrt{(M - I)^2 + 4p_o(p_o - I)}}{2} \tag{26}$$

In the undoped case the conductivity is

$$\sigma_o = e(n_o\mu_{eo} + p_o\mu_{ho}), \tag{27}$$

or $$\sigma_o = e\mu_{eo}(p_o - I_o) + e\mu_{ho}p_o \ ; \tag{28}$$

likewise in the doped case,

$$\sigma = e(n\mu_e + p\mu_h) \tag{29}$$

or $$\sigma = e\mu_e(p + M - I) + e\mu_h p \tag{30}$$

For simplicity, we let $\mu_{eo} = \mu_{ho} = \mu_e = \mu_h \equiv \mu$, and $I \cong I_o$;

then $$\sigma_o = e\mu(2p_o - I) \tag{31}$$

and $$\sigma = e\mu(2p + M - I) \ . \tag{32}$$

From Eq (26), we get

$$\sigma = e\mu \left(\sqrt{(M - I)^2 + 4p_o(p_o - I)}\right) \ ; \tag{33}$$

this and Eq (30) give

$$\sigma^2 - \sigma_o^2 = e^2\mu^2(M^2 - 2MI) = e^2\mu^2I^2[(\frac{M}{I})^2 - 2\frac{M}{I}] \qquad (34)$$

This result shows that the resistivity should increase as the metal concentration is increased until the metal concentration is approximately twice that of the edge ions. At that point the resistivity will begin to decrease toward the pure metal value. The data indicates that the metal ion concentration of the polymers of the highest doping level is not yet equal to twice the edge in concentration.

The above analysis assumes that the polymers are p-type semiconductors. The thermoelectric power measurements (Figure 12) show this to be the case. Table II gives the polymers, code names, room temperature resistivity (at 2kbar pressure), and other experimental parameters.

Electron spin resonance techniques were used to determine the unpaired spin concentration, S . It was hoped that some correlation between the resistivity and the spin density could be established. However, results (Figures 13 and 14) were of such an unreproducible and scattered nature that no correlation could be made. The bars of Figures 13 and 14 indicate the range of the spin concentrations determined by three repetitions of the measurements; the data point is an average value. It is seen that in all cases the spin concentration is quite high, and generally increases with increased doping level (Figure 15). Figure 16 depicts the spin concentration versus T^{-1} for a representative polymer. The irreproducibility and scatter of this data makes any spin activation energy only very approximate.

Resistivity data as a function of temperature was taken in two ranges: 300°K to 63°K, and 300°K to 1.7°K. Figures 17 and 18 show

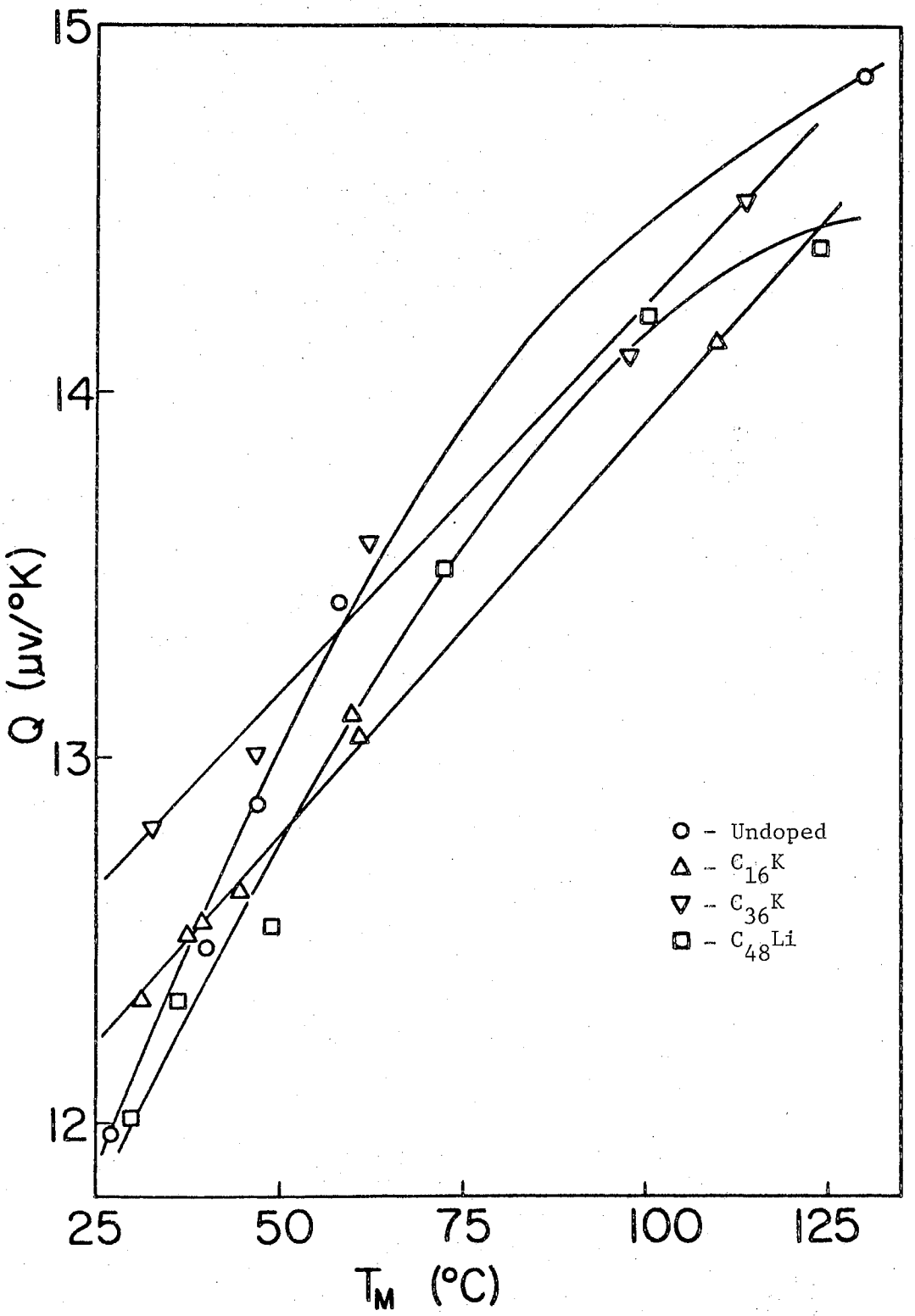

Figure 12. Q Versus T_M for 1000°C Potassium and Lithium Polymers
P = 2 kbar, T = 297°K

TABLE II

Heat Treatment Temperature, Code Name, Metal Concentration, Room Temperature Resistivity at 2 kbar, High Temperature Activation Energy, Low Temperature (Hopping) Activation Energy, Spin Concentration at Room Temperature, Thermoelectric Power at Room Temperature, Estimated Distance of Fermi Level Below Edge of Localized States for the Metal-Doped Pyropolymers.

Polymer	T_H (°C)	Code Name	At% M	$N_D \times 10^{21}$ (cm^{-3})	ρ (ohm-cm)	E_a (eV)	E_a' (eV)	S $\times 10^{19}$ (gm^{-1})	Q ($\mu v/°K$)	T_c (°K)	$E_c - E_F$ (eV)
C_8K	600	1A	11.1	8.9	9.6×10^{1}	0.083					
$C_{16}K$	600	2A	5.9	5.2	1.5×10^{3}						
$C_{24}K$	600	3A	4.0	3.7	4.2×10^{3}						
$C_{36}K$	600	4A	2.7	2.7	1.0×10^{4}						
C_8K	800	1B	11.1	8.9	8.9×10^{-1}	0.013	2.2×10^{-4}			62	5.3×10^{-3}
$C_{16}K$	800	2B	5.9	5.2	6.5×10^{-1}	0.008					
$C_{24}K$	800	3B	4.0	3.7	9.3×10^{-1}						
$C_{36}K$	800	4B	2.7	2.6	1.0						
C_8K	1000	1C	11.1	8.9	3.1×10^{-1}	0.004		11.0	12.1		
$C_{16}K$	1000	2C	5.9	5.2	2.6×10^{-1}	0.003	6.5×10^{-5}	8.8	12.2	43	3.7×10^{-3}
$C_{24}K$	1000	3C	4.0	3.7	1.2×10^{-1}	0.002		5.1	12.6		
$C_{36}K$	1000	4C	2.7	2.6	3.5×10^{-2}	0.002		6.2	12.9		
C_8K	1200	1D	11.1	8.9	3.7×10^{-1}	0.007		1.9			
$C_{16}K$	1200	2D	5.9	5.2	1.1×10^{-1}	0.001		9.1			
$C_{24}K$	1200	3D	4.0	3.7	7.3×10^{-2}	0.001		1.4			
$C_{36}K$	1200	4D	2.7	2.6	3.2×10^{-2}	0.001		1.6			
C_4Li	1000	13CA	20.0	21.9	1.9×10^{-1}	0.022	9.5×10^{-5}	3.5	13.1	58	5.0×10^{-3}
C_8Li	1000	13C	11.1	11.7	1.2×10^{-1}	0.006	8.2×10^{-5}	9.1	11.4	38	3.3×10^{-3}
$C_{16}Li$	1000	14C	5.9	6.1	3.3×10^{-2}	0.005	5.8×10^{-5}	11.0	11.6	50	4.3×10^{-3}
$C_{24}Li$	1000	15C	4.0	4.1	5.1×10^{-2}	0.005	5.0×10^{-5}	5.6	12.0	50	4.3×10^{-3}
$C_{51}Li$	1000	16C	1.9	1.9	1.9×10^{-2}	0.009	2.6×10^{-5}	5.0		16	1.4×10^{-3}
$C_{48}Li$	1000	17C	2.0	2.1	3.4×10^{-2}	0.006		3.8	11.9		
Undoped	600		0		1.2×10^{3}						
Undoped	800		0		3.7×10^{-1}						
Undoped	1000		0		1.3×10^{-2}			5.1	12.0		
Undoped	1200		0		1.2×10^{-2}						

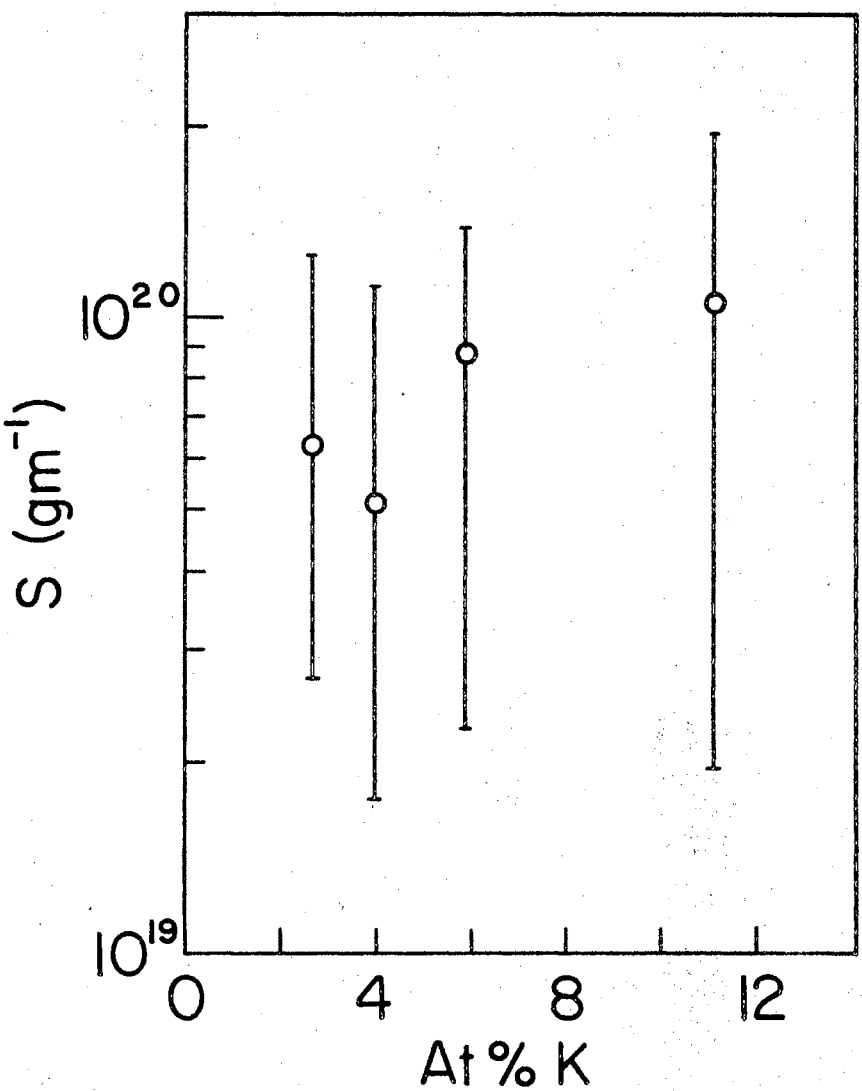

Figure 13. S Versus At% K for 1000°C Potassium Polymers Showing Dispersion in Results. T = 297°K

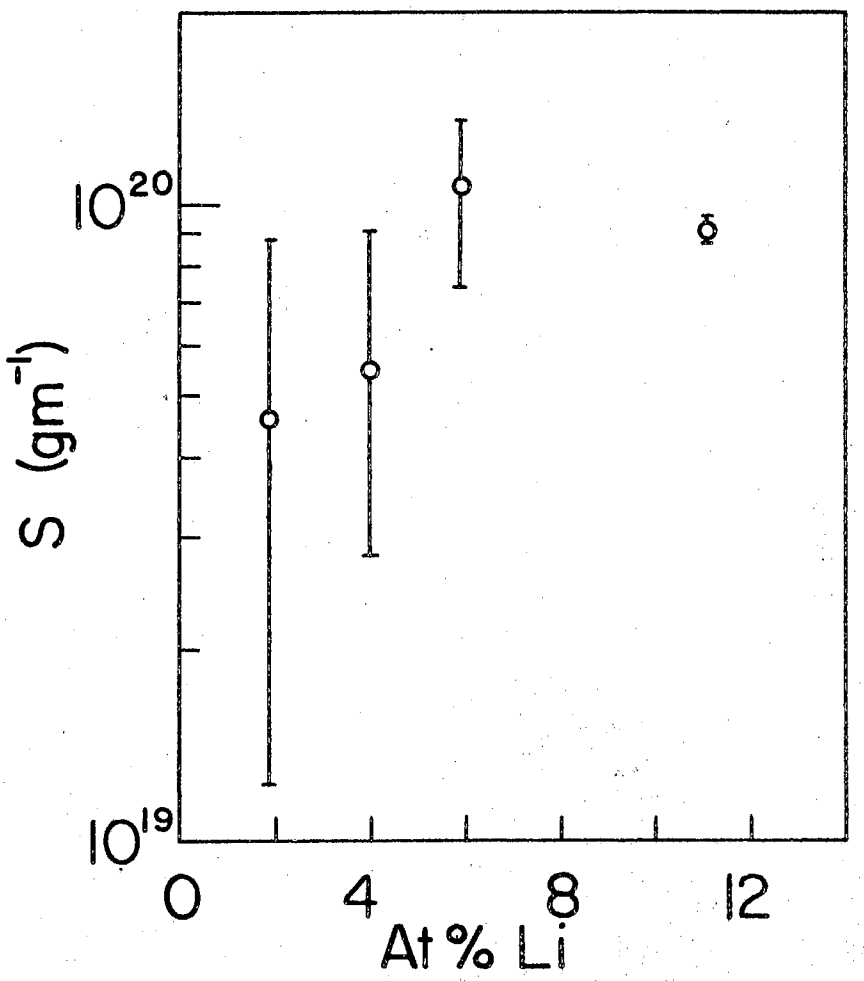

Figure 14. S Versus At% Li for 1000°C Lithium Polymers Showing Dispersion in Results.
T = 297°K

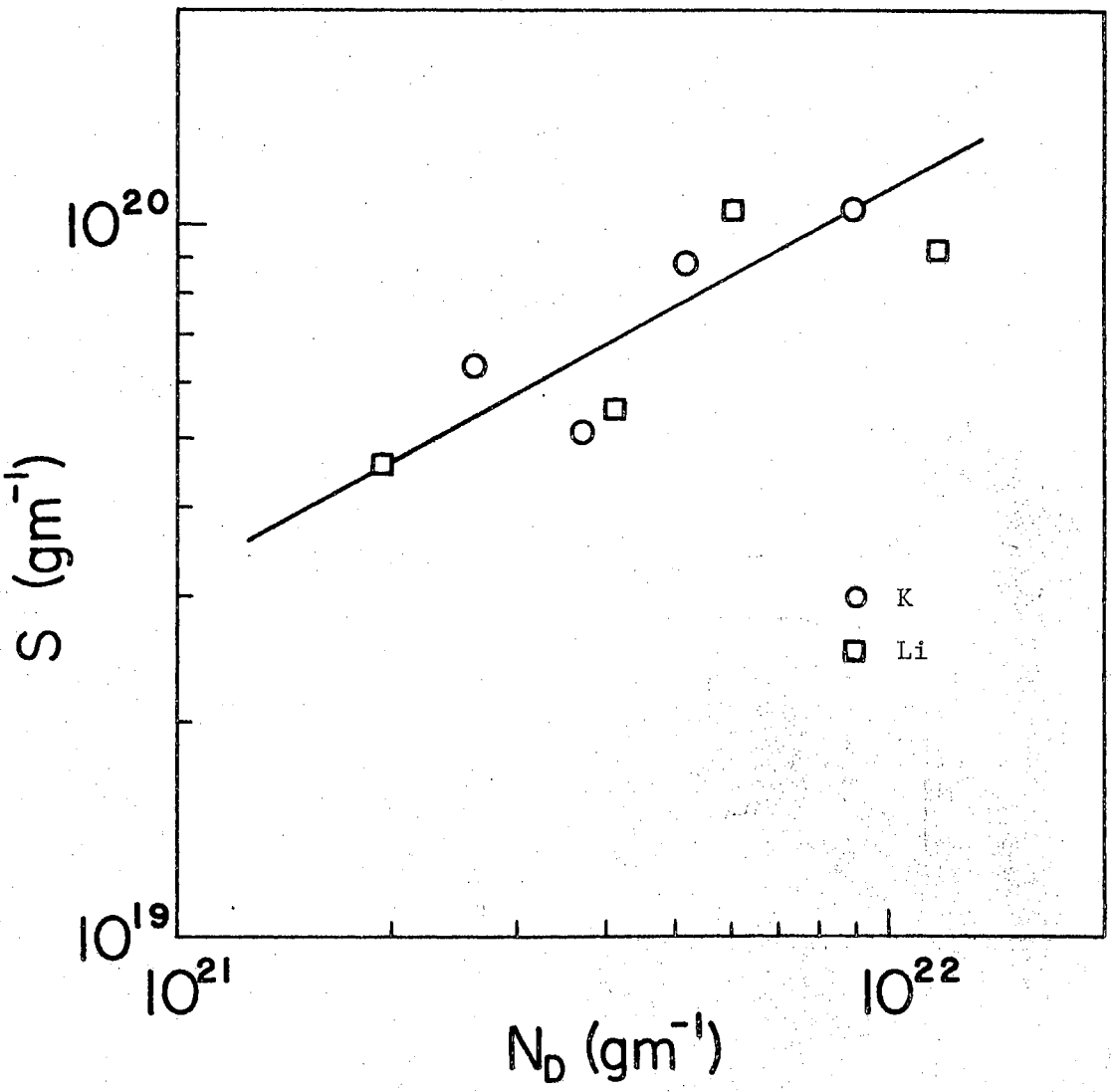

Figure 15. S Versus N_D for 1000°C Potassium and Lithium Polymers
T = 297°K

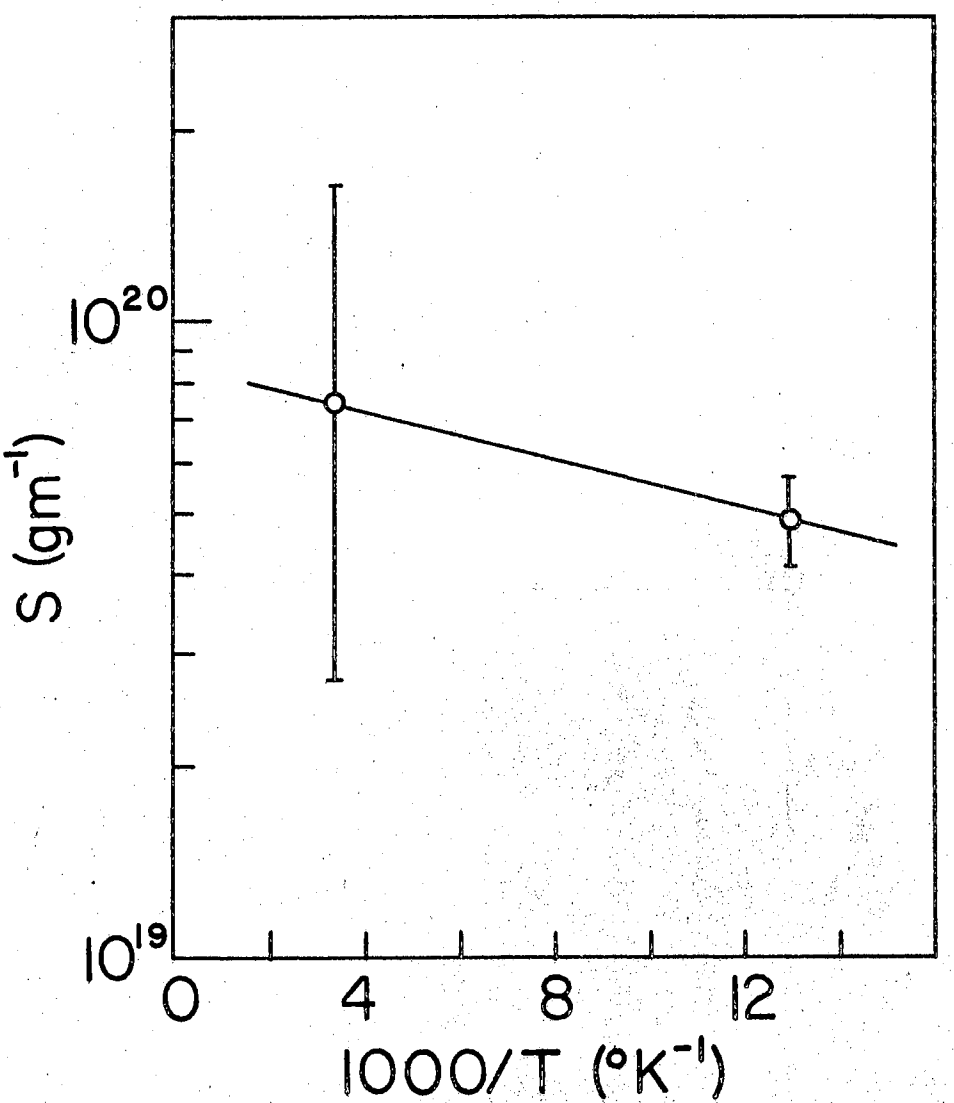

Figure 16. S Versus 1000/T for Polymer 14C showing Dispersion in Results

data for these two ranges. The slope of the lines in Figure 17 gives an activation energy, E_a .

The data of Figure 18 is similar to that of Spring-Thorpe, Austin and Austin (44) as quoted by Mott (45), and that of Fritzsche and Cuevas (46) in Mott (22). Cutler and Mott (21), following the theoretical lead of Anderson (40), propose a model of non-interacting electrons moving in a random potential created by charged defects.

The random potential tends to broaden the density of states, and creates a region of localized states in the low energy tail of the density of states. Here localization means that there is little overlap between the wave functions on the various centers; i.e., an electron in one of these states is trapped. These localized states are separated from the band region at energy E_c .

Clearly there are two possible cases: $E_F \geq E_c$ or $E_F < E_c$. If the first situation occurs, then the resistivity increases linearly as the temperature approaches zero and the localized states play no important part. However, for $E_F < E_c$ there will be states both above and below E_c . When $E > E_c$ there are band states available and band conduction dominates due to the high mobility of the band states. This corresponds to region I of Figure 18. As E decreases to and becomes less than E_c , the conduction mechanism changes to a hopping or tunneling transport. This is the mechanism of region III in Figure 18. In region II $E_F < E_c$ but $E_c - E_F < kT$ and there is a mixture of the two mechanisms; i.e., region II is a transition region. E_a' in Table II is the activation energy in region III.

Extrapolation of the lines in regions I and III defines a critical temperature, T_c , at their intersection. The energy kT_c gives an

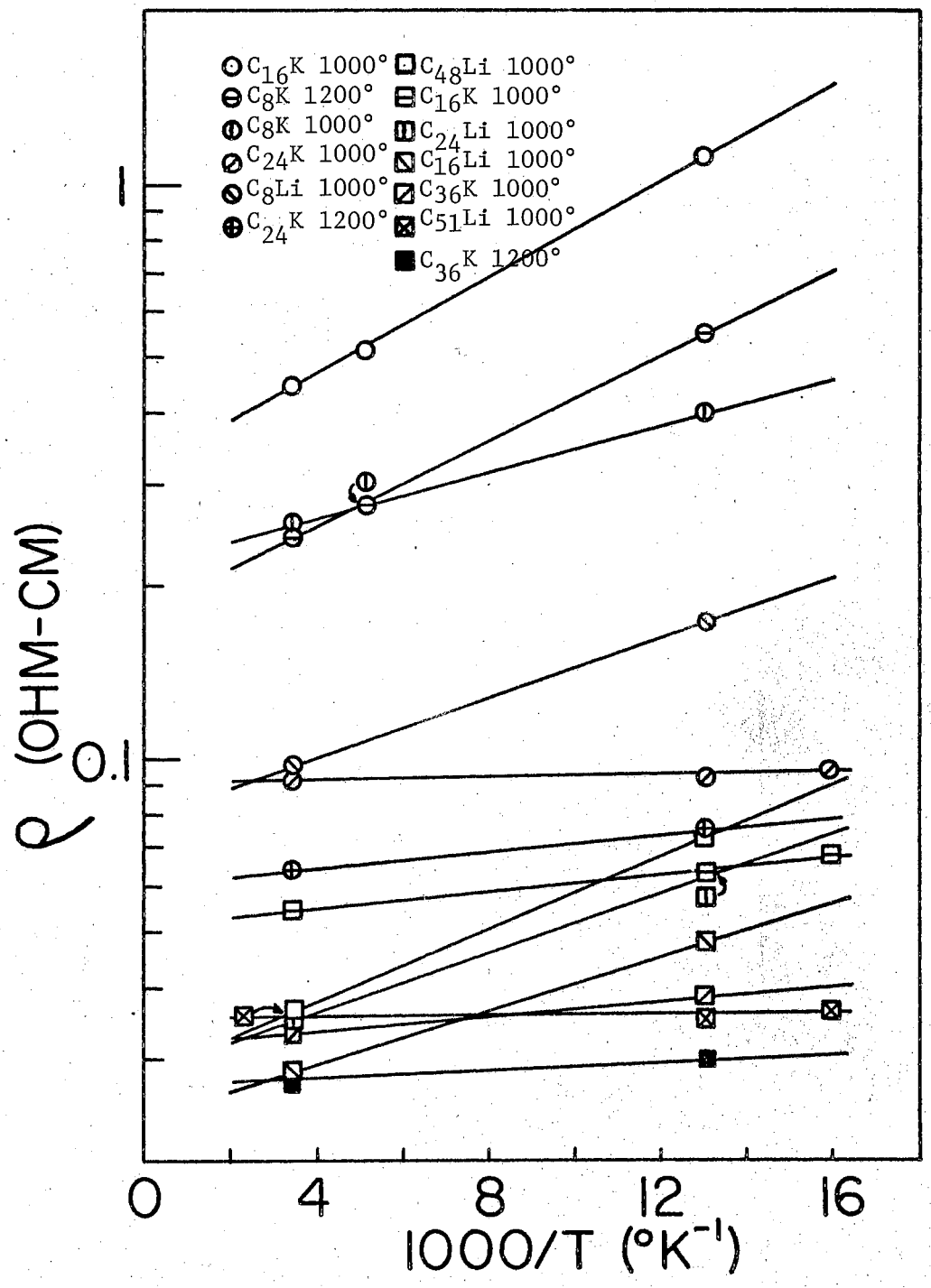

Figure 17. ρ Versus 1000/T for 13 Potassium-and Lithium-Doped Polymers in Temperature Range 300°K to 63°K. P = 2 kbar

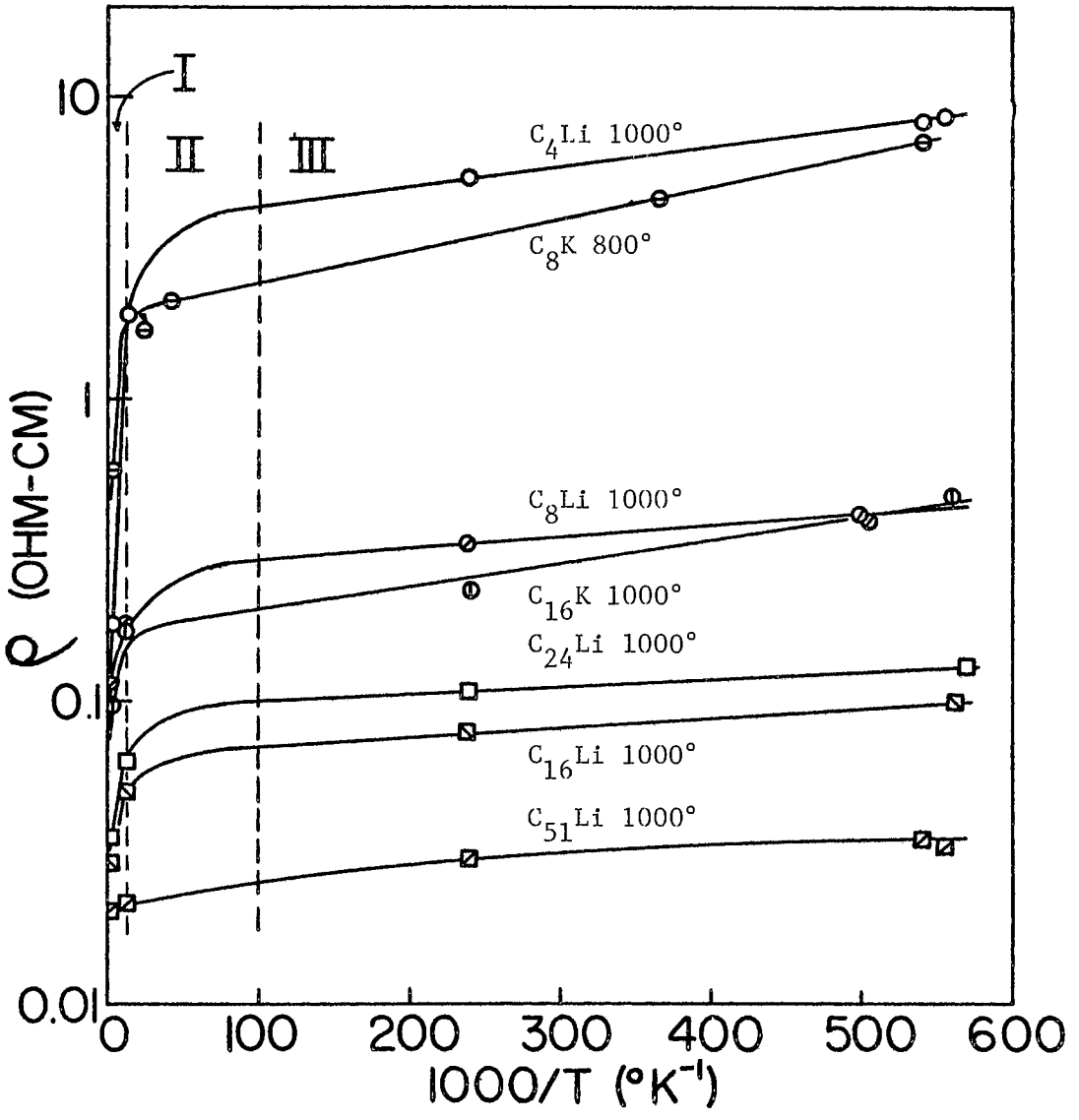

Figure 18. ρ Versus 1000/T for 7 Potassium-and Lithium-Doped Polymers in Temperature Range 300°K to 1.7°K
P = 2 kbar

estimation of $E_c - E_F$. The values of T_c and $kT_c = E_c - E_F$ are given in Table II.

Cutler and Mott (21) develop an expression for the isotropic conductivity in a band (47) as follows:

$$\sigma = -e^2 \int \frac{1}{3} \tau v^2 \left(\frac{\partial f}{\partial E}\right) N(E)\, dE \tag{35}$$

where τ is a scattering time, v a mean velocity, f the Fermi-Dirac function, and $N(E)$ the density of states. Using the relation

$$\frac{\partial f}{\partial E} = -\frac{1}{kT} f(1 - f) \tag{36}$$

and defining a mean free path or scattering distance, L, by

$$L^2 = \frac{1}{3}(\tau v)^2 \tag{37}$$

gives

$$\sigma = \int \frac{e^2 L^2}{2kT} f(1 - f)\, N(E)\, dE \tag{38}$$

A corresponding expression for the Seebeck coefficient is

$$S\sigma = -\frac{k}{e} \int \frac{e^2 L^2}{\tau kT} \left(\frac{E - E_F}{kT}\right) f(1 - f)\, N(E)\, dE. \tag{39}$$

These expressions give the current between two states, 1 and 2, due to an electric field $\mathcal{E}$ and a temperature gradient dT/dx as

$$j_{12} = \frac{ed}{\tau} \left[f_1(1 - f_2)e^{-\mathcal{E}ed/2kT} - f_2(1 - f_1)e^{\mathcal{E}ed/2kT}\right] \tag{40}$$

where d is the distance between the two states along the $\mathcal{E}$-field direction. f_1 and f_2 are the Fermi-Dirac functions at states 1 and 2; they differ from $f(T)$ by $\pm(dT/dx)(df/dT)(\frac{1}{2}d)$ at the average position of the two states. Expanding the exponentials and retaining only the linear terms in dT/dx and $\mathcal{E}$ gives

$$j_{12} = \frac{e^2 d^2}{\tau kT} f(1 - f) + \frac{k}{e}\left(\frac{e^2 d^2}{\tau kT}\right)\left(\frac{E - E_F}{kT}\right) f(1 - f)\frac{dT}{dx} \qquad (41)$$

Summing over all states at a given energy transforms $\frac{d^2}{\tau}$ to $(L^2/\tau)N(E)$. Then for $E > E_c$, L^2/τ corresponds to the diffusion constant for an electron gas. For $E < E_c$, L^2/τ is the diffusion constant for a random walk type of process. This is because the electron drift by the hopping mechanism is an electric field or temperature gradient is by a series of transitions between adjoining localized states of varying energy.

CHAPTER IV

SUMMARY, CONCLUSIONS AND SUGGESTIONS FOR FURTHER STUDY

Summary

In this study 22 potassium- and lithium-doped pyropolymers were studied to try to better understand the electrical transport mechanism in non-crystalline solids. In order to study the polymers a method was developed to measure the electrical properties by a four-point probe arrangement under pressures of up to 2.5 kbar.

Resistivity as a function of pressure data indicates that bulk properties were being measured. This data plus the resistivity as a function of doping level and the x-ray data indicates that the materials are compounds, not mixtures, of carbon and the metal. Thermoelectric power measurements were used to show that the polymers were p-type materials with absolute thermoelectric powers of from 11.4×10^{-6} v/°K to 13.1×10^{-6} v/°K.

Resistivity was measured as a function of temperature between 300°K and 1.7°K. In the temperature range between 300°K and ~63°K the polymers behaved as band-type semiconductors with activation energies between 0.001 eV and 0.083 eV. However, in the lower range, from ~63°K to 1.7°K, the polymers underwent a transition from the band-like to a tunneling mechanism. This indicated the formation of localized

states in the low energy tail of the density of states due to the random nature of the charged impurity centers. The Fermi level was from ~1.4 x 10^{-3} eV to ~5.3 x 10^{-3} eV below the edge of the localized states. The tunneling mechanism has an activation energy, E_a', of between 2 x 10^{-5} eV to 2 x 10^{-4} eV.

Conclusions

The metal-doped pyropolymers studied are p-type semiconductors with resistivities between 1 x 10^{4} ohm-cm and 2 x 10^{-2} ohm-cm. Evidence indicates that the materials are compounds with empirical formula C_xM, where x ranges from 4 to 51 and M is potassium or lithium.

Resistivity-temperature data in the temperature range of 300°K to 1.7°K reveals an anomolous behavior. This is attributed to a transition between band-like conduction and a tunneling mechanism. This indicates that localized states have been formed due to the presence of a random impurity potential, and that the Fermi energy is below the edge of the localized states.

Suggestions for Further Study

More insight into the conduction mechanism of the polymers might be gained by the following further studies. More detail in the resistivity-temperature data would be helpful, especially in the range of 60°K to 4.2°K. This would give more accurate data about the transition and density of states near the transition. Also Seebeck measurements at low temperatures could be correlated with the resistivity. AC measurements giving dielectric constants, relaxation times, and conductivities,

would be useful in determining the details of the mechanism.

BIBLIOGRAPHY

1. Krishnan, K. Nature 144, 667(1939).

2. Coulson, C. Nature 159, 265(1947).

3. Wallace, P. Phys. Rev. 71, 622(1947).

4. Bowen, D. Phys. Rev. 76, 1878(1949).

5. Mrozowski, S. Phys. Rev. 77, 838(1950).

6. McDonnell, F., R. Pink, and A. Ubbelohde, J. Chem. Soc. Pt. 1, 191(1951).

7. Hennig, G. J. Chem. Phys. 19, 922(1951).

8. Mrozowski, S. J. Chem. Phys. 21, 492(1953).

9. Pohl, H. Proc. Fourth Carbon Conf., Ed. S. Mrozowski (Pergamon Press, New York, 1960), p.

10. Pohl, H., and J. Laherrere, Proc. Fourth Carbon Conf., Ed. S. Mrozowski (Pergamon Press, New York, 1960), p. 259.

11. Pohl, H., and S. Rosen, Proc. Fifth Carbon Conf., Vol. II, (Pergamon Press, New York, 1963), p. 113.

12. Pohl, H. and J. Laherrere, Princeton Univ. Plastics Lab. Tech. Report 57C, April 15, 1960.

13. Chambers, R. and J. Park, Brit. J. Appl. Phys. 12, 507(1961).

14. Pohl, H., A. Rembaum, and A. Henry, J. Am Chem. Soc. 84, 2699(1962).

15. Pohl, H. and D. Opp, J. Phys. Chem. 66, 2121(1962).

16. Mott, N., Proc Phys. Soc. A62, 416(1949).

17. Mott, N. Phil. Mag. 6, 287(1961).

18. Mott, N. Rev. Mod. Phys. 40, 677(1968).

19. Miller, A., and E. Abrabams, Phys. Rev. 120, 745(1960).

20. Cutler, M., and J. Leavy, Phys. Rev. 133, A1153(1964).

21. Cutler, M. and N. Mott, Phys. Rev. 181, 1336(1969).

22. Mott, N. Contemp. Phys. 10, 125(1969).

23. Mott, N. Phil. Mag. 17, 1259(1968).

24. Mott, N. Adv. Phys. 18, 41(1969).

25. Lifshitz, I. Adv. Phys. 13, 483(1967).

26. Böer, K. Phys. Stat. Sol. 34, 721(1969).

27. Böer, K. Phys. Stat. Sol. 34, 733(1969).

28. Böer, K. J. Non-Cryst. So. 2, 444(1970).

29. Ottmers, D. and H. Rase, Carbon 4, 125(1966); see also H. Podall, W. Foster, and A. Giraitis, J. Org. Chem. 23, 82(1958).

30. Pohl, H. Modern Aspects of the Vitreous State, Vol. II. Ed. J. D. Mackenzie (Butterworths, London, 1962), p. 72.

31. Pohl, H. Proc. Fourth Carbon Conf., Ed. S. Mrozowski (Pergamon Press, New York, 1960), p. 243.

32. Bridgman, P. W. Collected Experimental Papers (Harvard Press, Cambridge, 1967).

33. Gutmann, F. and L. Lyons, Organic Semiconductors (John Wiley and Sons, Inc., New York, 1967), p. 58.

34. van der Pauw, L. Philips Res. Repts. 13, 1(1958).

35. Chester, P. and G. Jones, Phil. Mag. 44, 1281(1953).

36. See, e.g., W. Schockley, Electrons and Holes in Semiconductors (D. van Nostrand, New York, 1950).

37. Hartman, R. Ph.D. Thesis, Oklahoma State University, Stillwater, Oklahoma, 1968.

38. Alger, R. S., Electron Paramagnetic Resonance: Techniques and Applications (John Wiley and Sons, Inc., New York, 1968).

39. See, e.g., X-ray Diffraction by Polycrystalline Material, Ed, H. S. Peiser, H. P. Rooksby, and A. J. C. Wilson (John Wright and Sons, Ltd., London, 1955), or X-ray Diffraction Procedures for Polycrystalline and Amorphous Materials, H. P. Klug and L. E. Alexander (John Wiley and Sons, Inc., New York, 1954), p. 491.

40. Anderson, P. Phys. Rev. 109, 1492(1958).

41. Private Communication, J. R. Wyhof.

42. Winslow, F., W. Baker, N. Pape, and W. Matreyek, J. Poly. Sci. 16, 101(1955).

43. Noda, T., M. Inagaki, and S. Yamada, J. Non-Cryst. Sol. 1, 285(1969).

44. Spring-Thorp, A., I. Austin, and B. Austin, Solid St. Comm. 3, 143(1965).

45. Mott, N., J. Non-Cryst. Sol. 1, 1(1968).

46. Fritzsche, H., and M. Curvas, Phys. Rev. 119, 1238(1968).

47. See, e.g., Electrons and Phonons, J. M. Ziman (Oxford University Press, Oxford, 1960).

VITA

Steven David Hottman

Candidate for the Degree of

Master of Science

Thesis: SEMICONDUCTION IN METAL-DOPED PYROPOLYMERS

Major Field: Physics

Biographical:

Personal Data: Born in Abilene, Kansas, February 24, 1947, the son of David and Margaret Hottman; married Susan Crow Hottman, January 18, 1969.

Education: Attended high school in Abilene, Kansas; was graduated from C. E. Donart High School in Stillwater, Oklahoma, in 1965; received Bachelor of Science degree from Oklahoma State University, with a major in Physics, in May, 1969; completed the requirements for the Master of Science degree in July, 1970.